Journal of Agricultural Science; Vol. 15, No. 4; 2023
ISSN 1916-9752 E-ISSN 1916-9760
Published by Canadian Center of Science and Education

Remote Sensing and Aerodynamic Temperature-Based Energy Balance Models to Estimate Crop Evapotranspiration Rates

José L. Chávez[1]

[1] Civil and Environmental Engineering Department, Colorado State University, Fort Collins, Colorado, USA

Correspondence: José L. Chávez, Civil and Environmental Engineering Department, Colorado State University, 1372 Campus Delivery, Fort Collins, Colorado, 80523, USA. Tel: 1-970-491-6095. E-mail: jose.chavez@colostate.edu

Received: January 22, 2023 Accepted: February 19, 2023 Online Published: March 15, 2023

doi:10.5539/ URL: https://doi.org/10.5539/

The research is financed by the National Science Foundation.

Abstract

Different methods exist to measure or estimate actual crop evapotranspiration (ET_a). However, some methods require a large number of data input or strict field conditions. Remote sensing based ET_a algorithms based on extreme thermal pixels (hot and cold) have limitations when required extreme pixels are not present in the acquired thermal infra-red imagery. In addition, satellite overpass frequency and spatial pixel resolution may be a limitation for some agricultural fields and micro-climates. Surface energy balance methods that use surface radiometric temperatures often fail to perform well under drought, limited irrigation, salt affected soils, or under sparse vegetation conditions. One option is to measure or estimate the crop/surface sensible heat flux through the aerodynamic temperature approach, then calculate the available energy and solve the energy balance for latent heat flux. Thus, this study presents different published algorithms that characterize the crop or field surface aerodynamic temperature and then applies them to different conditions for evaluation. Determining spatial ET_a continuously has the potential to improve the irrigation water management decision making. The aerodynamic temperature approach was initially developed with good results as a function of surface radiometric temperature, air temperature, crop leaf area index, and wind speed or surface aerodynamic resistance. However, the inclusion of the crop fractional percent cover and of a new resistance term (turbulent-mixing row resistance) greatly improved the estimation of the sensible heat and latent heat fluxes, when evaluated with heat flux data derived from eddy covariance energy balance towers. Results also indicate that the aerodynamic method has transferability potential to different regions, crops, and irrigation methods than the conditions encountered in the method development.

Keywords: irrigation management, actual crop water use, remote sensing, evapotranspiration, energy balance

1. Introduction

Increasing world population and climate change demand a global sustainable food and fiber production under well managed irrigation practices. Thus, the need to become more efficient at managing water resources in agricultural settings and at different spatial scales. In this context, remote sensing (RS) systems along with actual crop water use or evapotranspiration (ET_a, mm d^{-1}) algorithms can be implemented to improve irrigation management decisions (Chávez et al., 2012, Gowda et al., 2008). One such ET_a estimation method is based on the energy balance (EB) approach that provides instantaneous estimates of latent heat flux (LE, W m^{-2}), at the time of satellite platform overpass, and which is converted to hourly and daily actual evapotranspiration using different time-steps scaling methods (Chavez et al., 2008). The simplified EB approach is defined by the equation "$R_n = G + H + LE$," where R_n is net radiation, G is the soil heat flux, and H is sensible heat flux. All EB terms are expressed in W m^{-2} units in this study. Appendix A lists the calcuations needed to estimate R_n and G for the typical EB approach used in this study. The estimation of LE is performed by solving the EB equation for LE after estimating R_n, G, and H. R_n and G are estimated with acceptable accuracy (~95% and 85%, respectively). There are several RS algorithms available (Gowda et al., 2008) to estimate these variables. However, most RS and EB based ET_a algorithms differ in the way the sensible heat flux is estimated. In most of these models, H is estimated using the radiometric surface temperature (T_s), derived from satellites' thermal bands or ground-based radiometry. Sensible heat fluxes are in

general over estimated when T_s is used in Equation 1 rather than the appropriate surface aerodynamic temperature (T_o). Equation 1 below describes the bulk surface resistance-based H calculation. The over estimation of H often occurs because T_s is typically larger than T_o.

$$H = \rho_a \cdot Cp_a \cdot (T_o - T_a)/r_{ah} \quad (1)$$

where, ρ_a is air density, (kg m^{-3}), Cp_a is specific heat of dry air 1005 (J kg^{-1} K^{-1}), T_a is air temperature (K) at screen height (2-3 m). The surface aerodynamic temperature (T_o, K) is defined as the within and between canopy temperature that produces the necessary temperature gradient for the generation of sensible heat fluxes. For homogeneous canopies T_o can be said to originate at the height equal to the zero plane displacement (d, m) plus the roughness length for heat transfer (Z_{oh}, m). In Equation 1, r_{ah} is the surface aerodynamic resistance, (sec m^{-1}) to heat transfer from a height equal to "d+Zoh" to Z_m. Where Z_m is the wind speed measurement height, m.

Wenbin et al. (2004) indicated that for homogeneous and isothermal surfaces the definition of aerodynamic and thermodynamic (canopy or surface radiometric) temperatures are equivalent, but over heterogeneous (and/or sparse, or stressed) surfaces there are important differences between T_o and T_s. This difference leads to errors in the estimation of H which in turn leads to errors in the calculation of LE and therefore in mapping ET_a. In order to account for the differences between T_o and T_s, studies have been carried out to parameterize H. For instance, earlier studies by Kustas et al. (1989), and Kustas and Norman (1996) increased the surface aerodynamic resistance by adding an extra term that adjusts the surface roughness length for heat transfer. This term expresses the extra resistance that the heat flow encounters above the vegetation canopy in relation to the momentum flux. Chehbouni et al. (1996), introduced a β parameter as function of leaf area index (LAI, m^2 m^{-2}) in an exponential relationship, in the H equation, to adjust for the differences between T_o and T_s.

Since those early studies, further research has been carried out to model and apply the surface aerodynamic temperature approach; in particular, using input data from different RS platforms. Therefore, this article summarizes different surface aerodynamic temperature modeling studies and applies selected T_o models to different crops, regions, and irrigation conditions to assess their transferability.

2. Method

This section introduces several surface aerodynamic temperature models that used different remote sensing platforms (sensors and spatial scales). Then, selected T_o models are applied to: a) a cotton field near Bushland, Texas; b) a maize field located near Rocky Ford, Colorado; and to c) a maize field in Fort Collins, Colorado.

2.1 Maize and Soybean T_o Modeling—Rainfed Agriculture Case

Mahrt and Vickers (2004), for grass, modeled T_o in terms of T_s, incoming shortwave solar radiation (R_s, W m^{-2}), a vegetation index (or leaf area index, LAI), horizontal wind speed (U, m s^{-1}) and soil water content. Similarly, Chávez et al. (2005) modelled T_o (°C) as a multi-linear regression function of T_s, T_a, LAI, and U, for dryland maize and soybean crops located near Ames, Iowa, USA. Equation 2 below shows the resulting multiple linear regression T_o model, where surface reflectance and temperature images were obtained using multispectral/thermal cameras mounted on an aircraft (1-3 m pixel spatial resolutions). These images were used to determine LAI and T_s, respectively. The validity of Equation 2 is for a range of LAI between 0.3 and 5.0 m^2 m^{-2}.

$$T_o = 0.534 \cdot T_s + 0.39 \cdot T_a + 0.224 \cdot LAI - 0.192 \cdot U + 1.67 \quad (2)$$

Equation 2 above resulted with the following mean bias error (MBE) and root mean square error (RMSE) of 0.2 and 0.9 °C, respectively, when evaluated with T_o derived from inverting Equation 1 and using sensible heat fluxes measured with a network of Eddy Covariance (EC) EB systems. Further, when using T_o from Equation 2 in Equation 1 and solving the EB equation for the latent heat flux, LE was estimated with a relatively small error (MBE±RMSE) of -9.2±39.4 W m^{-2} or -2.7±11.7% (relative or normalized error), when evaluated with LE from EC EB towers.

2.2 Cotton T_o Modelling—Dryland Agriculture Case

In a study over rainfed cotton subjected to a highly advective environment, in the Texas High Plains, near Bushland, Texas, USA, Chávez et al. (2010) modelled T_o (°C) using "inverted" T_o from 15-minute measured ET_a, R_n, and G data. These variables were measured at a precision monolithic weighing lysimeter field (210 m long × 200 m wide), and by solving the EB equation for H as a residual and by inverting Equation 1 and solving it for T_o. The form of the resulting T_o equation is shown below as Equation 3, with variables and corresponding units as previously defined. In Texas, the rainfed cotton was water stressed and LAI only varied from 0.2 to 1.3 m^2 m^{-2}. In this study, T_s was measured with a fixed Exergen infra-red thermometer, and crop height and LAI were estimated using

surface/vegetation reflectance data collected with an EXOTECH hand-held multispectral radiometer. Further details regarding the experiment setup can be found in Chávez et al. (2010).

$$T_o = 0.5 \cdot T_s + 0.5 \cdot T_a + 0.15 \cdot r_{ah} - 1.4 \quad (3)$$

The evaluation of T_o from Equation 3 was performed with T_o data from an aerodynamic profile tower (APT) and an EC EB system. The evaluation yielded the following errors, MBE±RMSE of 0.16±1.02 °C or 0.13±3.77% and 0.67±2.14 °C (2.24±6.53%), for the APT and EC reference systems, respectively. This small error in the estimation of T_o (Equation 3) contributed to a better estimation of dryland cotton ET_a rates, with an error reduction from 23.6 to 3% when T_o was used in Equation 1 instead of T_s.

2.3 Merlot Vineyard T_o Modelling—Irrigated Agriculture Case

Another study was carried out to calibrate and validate the surface aerodynamic temperature method for the estimation of the spatial variability of the sensible and latent heat fluxes over a drip-irrigated merlot vineyard located in the Maule Region, in Chile, South America. Figure 1 shows the merlot vineyard site that was instrumented with an EC EB system along with ancillary sensors.

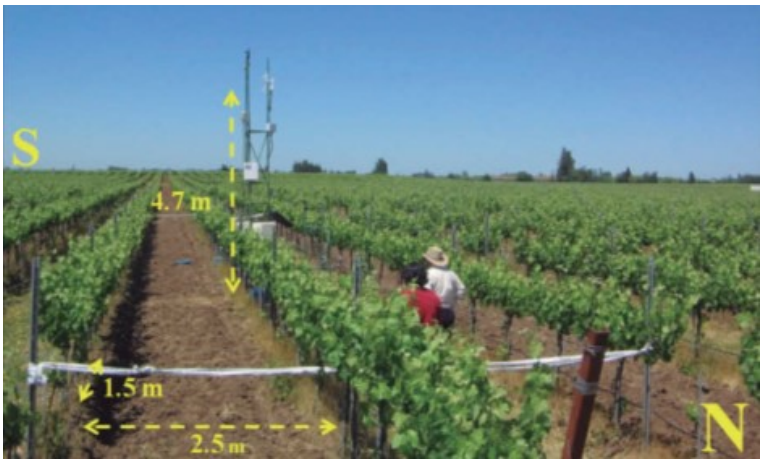

Figure 1. Merlot vineyard located in the Maule Region of Chile (35°25′ South and 71°32′ West, 125 m above mean sea level)

Source: Carrasco-Benavides et al. (2017).

The T_o calibration study was carried out by Carrasco-Benavides et al. (2017). For this study, measurements of EB components and meteorological data were collected during the 2006-2010 crop growing seasons. The experimental plot was composed of a 4.25 ha Merlot vineyard, which was equipped with an EC EB system and an automatic weather station. In this study, T_o was modelled in a similar fashion as indicated in Chávez et al. (2005), resulting in Equation 4 below. However, the RS data used were from satellite Landsat 7 optical/NIR and thermal images; which pixel spatial resolutions were 30 and 100 m for the multispectral and thermal images, respectively. The validity of Equation 4 is for a range of LAI and fractional vegetation cover values falling between 0.8-1.2 m^2 m^{-2} and 28-31%, respectively.

$$T_o = 0.2 \cdot T_s + 0.75 \cdot T_a + 24.46 \cdot LAI - 0.95 \cdot U - 22.77 \quad (4)$$

The evaluation of Equation 4 was performed with EC-derived (inverted) T_o values not used in the development of the vineyard T_o model. The evaluation indicated that Equation 4 estimated T_o with the following errors, MBE±RMSE of 0.56±0.66 °C or 2.3±2.7%. Further, the resulting sensible heat flux estimation error was 28.3±33.6 W m^{-2} or 10.5±12.4%; while satellite data-based computations of LE were somewhat higher than those EC-based measured at the time of satellite overpass (53±63 W m^{-2} or 28.3±33.6%), presumably due to the biases embedded in the net radiation and soil heat flux computations, according to Carrasco-Benavides et al. (2017). However, the proposed RS-based EB method to estimate ET_a based on T_o is very simple to implement, presenting similar accuracies on ET_a mapping than those computed by complex satellite-based EB models.

2.4 Maize T_o Modelling—Irrigated Agriculture Case

A recent study, by Costa-Filho et al. (2021), modelled T_o over maize fields (fully and deficit sub-surface drip irrigated) near Greeley, Colorado, USA, using proximal RS data collected with handheld and fixed ground-based

radiometers, and with sensible heat fluxes measured with two sets of Large Aperture Scintillometers (LAS) that provided T_o values (from inverted measured H values). Rambikur and Chávez (2014) presented a LAS evaluation study in which it was shown that sensible heat fluxes derived from LAS systems were comparable to H values obtained with EC systems. In the Costa-Filho et al. (2021) study, T_o was modelled for different ranges of maize LAI values including the following variables: fractional vegetation cover (f_c), T_s, T_a, and considering the wind direction (angle) interaction with the crop rows' orientation (angle) through the so-called 'turbulence mixing-row resistance' (r_p, s m^{-1}). Wind direction has a significant effect on determining the wind profile within and above canopy relative to air flow direction and the crop row layout. As wind speed interacts with the crop row orientation (wind from different directions), there will be different angles of attack that will result in different aerodynamic resistances and wind penetration within the crop (*i.e.*, variable zero-plane displacement height and roughness length); which results in different turbulent mixing of heat and vapor transport from the surface to the atmosphere above affecting H and LE fluxes. Below, Equations 5-8 present Costa-Filho et al. (2021) modelled T_o equations for maize grown in a high plain and semi-arid region.

$$T_o = -8.742 \cdot f_c + 0.571 \cdot T_a + 0.529 \cdot T_s + 0.806 \cdot r_p + 3.295 \quad \text{for } 0.85 \leq LAI \leq 1.50 \tag{5}$$

$$T_o = -9.168 \cdot f_c + 0.485 \cdot T_a + 0.575 \cdot T_s - 0.160 \cdot r_p + 6.491 \quad \text{for } 1.5 < LAI \leq 2.50 \tag{6}$$

$$T_o = 4.708 \cdot f_c + 0.350 \cdot T_a + 0.580 \cdot T_s + 0.086 \cdot r_p \quad \text{for } 2.50 < LAI \leq 3.50 \tag{7}$$

$$T_o = -1.912 \cdot f_c + 0.443 \cdot T_a + 0.509 \cdot T_s + 0.115 \cdot r_p + 5.014 \quad \text{for } 3.50 < LAI \leq 5.00 \tag{8}$$

The Costa-Filho et al. (2021) T_o resulting modelling errors (MBE±RMSE) were -0.14±0.50 °C for the optimized models (Equations 5-8). Overall, results seemed to indicate that the optimized T_o model improved the estimation of maize H fluxes (error -6±19 W m^{-2}, or -4.9±16.3%); which resulted in an improvement of the estimation of latent heat fluxes (error -6±35 W m^{-2}, or -1.8±9.7%). It seems that incorporating the interactions between the crop row layout and wind direction, in the modelling of T_o, better describes the dynamic turbulent mixing for the generation of H.

2.5 Application of T_o Models

Selected T_o models were applied to crops and conditions different from those used in their development. The T_o application was performed to assess the transferability of the models to different settings.

2.5.1 Applying the Chávez et al. (2005) Rainfed Maize T_o Model to Sprinkler Irrigated Cotton

Field data were collected in 2008 at the United States Department of Agriculture (USDA) Agricultural Research Service (ARS) Conservation and Production Research Laboratory (CPRL), located near Bushland, Texas, USA. The geographic coordinates of the USDA ARS CPRL are 35°11′ North and 102°6′ West, with an elevation of 1,170 m above mean sea level (amsl). The study area is subject to very dry air and strong winds (advection). Annual averages for air temperature, air water vapor pressure deficit, and horizontal wind speed are 14 °C, 0.3 kPa, and 4.9 m s^{-1}, respectively, according to Chávez et al. (2009).

Cotton was grown in a 4.7 ha research field (southeast lysimeter field) 210 m wide (East–West) and 225 m long (North-South). The field contained a precision weighing lysimeter in the center (Figure 2). The lysimeter measurements are 3.9 m wide × 3.9 m long × 2.3 m deep and it was used to directly measure cotton ET_a for the evaluation of the ET_a estimated with the T_o approach. The lysimeter contained a monolithic Pullman clay loam soil core and it was sprinkler irrigated by a Linear Move sprinkler irrigation system.

Figure 2. Cotton field with instrumentation installed above the lysimiter box, at the USDA ARS CPRL, Bushland, Texas, USA

For the application of Equation 2, T_s was obtained from infrared thermometers (model IRT/c, Exergen Corp., Watertown, Massachusetts, USA), which were mounted to view approximately at a 60° zenith angle and an azimuth toward the Southwest at 45° from due South. T_a was obtained from a temperature/relative humidity sensor (model HMP45C, manufactured by Vaisala, Inc.,) mounted in a Gill shield (model 41003-5 10-Plate Gill radiation shield manufactured by R.M. Young, Traverse City, Michigan, USA) at 2 m above the ground. Wind speed (U) was measured by an anemometer (model 03101-L R.M. Young wind sentry anemometer, manufactured by R.M. Young, Traverse City, Michigan, USA) at 2 m above the ground. And LAI was estimated as published in Chávez et al. (2010). The normalized difference vegetation index (NDVI) was calculated using surface reflectance data obtained with an EXOTECH handheld radiometer.

2.5.2 Applying the Chávez et al. (2005) Rainfed Maize T_o Model to Furrow Irrigated Maize

The study was conducted at the Colorado State University (CSU) Arkansas Valley Research Center (AVRC) near Rocky Ford, Colorado, USA. The geographic coordinates of the site are 38°2′ North and 103°41′ West, and the elevation is 1,274 m amsl. Maize was grown in the large lysimeter field (Figure 3) in 2013. The dimension of the large lysimeter field are 160 m by 250 m (4 ha). A large monolithic weighing lysimeter (3 m long × 3 m wide × 2.4 m deep) was located in the middle of the field. As part of the instrumentation in the field, there was a net radiometer (Q7.1, REBS, Seattle, Washington, USA), two infra-red thermometers (IRT Apogee model SI-111, CSI, Logan, Utah, USA) to measure crop radiometric surface temperature, soil heat flux plates (REBS model HFT3, CSI, Logan, Utah, USA) buried in the ground in the lysimeter box, 10 cm deep, along with soil temperature and soil water content sensors, for the estimation of stored soil heat and G at the ground surface. The field was furrow irrigated using siphons and a head ditch. The average annual maximum temperature is 21.1 °C. The average annual minimum temperature is 2.4°C. The long-term average annual precipitation at the site is 301 mm with approximately two-thirds of the annual total occurring from May through September. The total average annual snowfall is 589 mm.

Figure 3 shows a grid (light green dots) where ground-based multispectral/thermal radiometric data were collected over a span of 9 weeks (once a week).

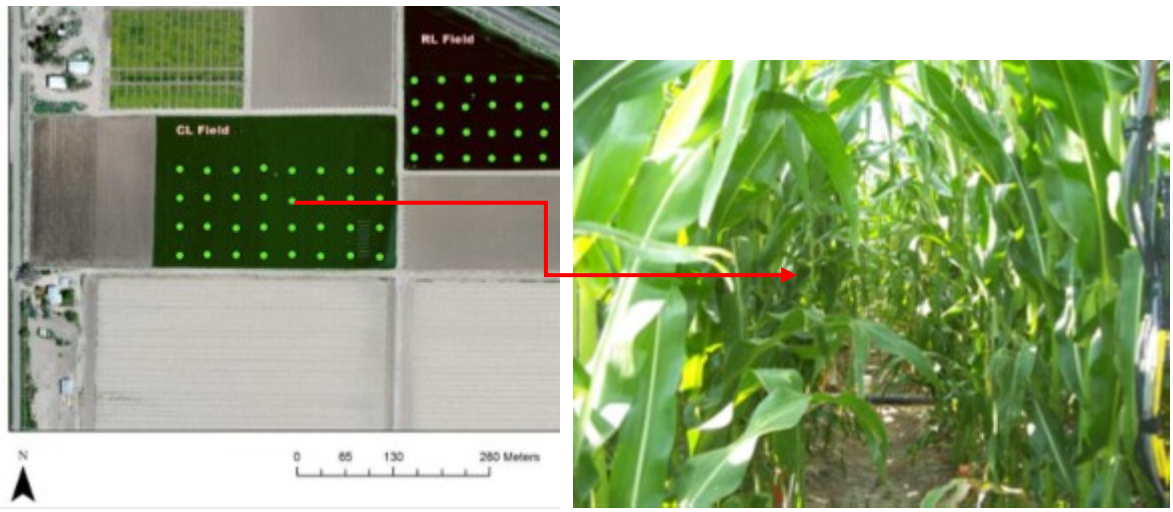

Figure 3. Maize field at the CSU AVRC lysimeter (CL) field near Rocky Ford, Colorado, USA

These radiometric data were used to obtain surface reflectance and temperature, respectively. A weather station was installed at the middle of the field, from where air temperature, relative humidity, and wind speed data, at 3 m above ground, were obtained.

Maize Fontanelle 8A818RBC was planted on May 7th with a density of 81,382 plants/ha. Emergence took place on May 17th, while the harvest occurred on October 15th.

The EB method based on T_o from Equation 2 was applied to the maize data collected at the lysimeter field.

2.5.3 Applying the Costa-Filho et al. (2021) Drip Irrigated Maize T_o Model to Furrow Irrigated Maize

The newer T_o model was applied to furrow irrigated maize grown at the Irrigation Innovation Consortium (IIC) Head Quarters (HQ). The IIC-HQ was located at the intersection of Prospect Road and Interstate-25 highway on the outskirts of Fort Collins, Colorado, USA. The site elevation is 1,525 m amsl, Lat. 40.557270 North and Long. -105.004932 West. The research field used was approximately 6.9 ha (348 m long × 200 m wide) located at the south-west (SW) corner of the site (Figure 4). Maize (Syngenta G02K39-3120) was planted on May 13, 2020, with a density of 81,500 plants/ha. Soil texture is Otero sandy loam. The climate is cold and temperate according to the Köppen-Geiger climate classification. The irrigation system was furrows, supplied of water by siphons (every other furrow) from a head ditch. An EC tower (CSI, Logan, Utah, USA) was installed at the northwest corner of the field in order to evaluate the T_o-based ET_a estimates. A net radiometer, soil heat flux plates, and IRTs were installed in the upper one-third of the field to assess available energy and the EC EB closure.

PlanetScope high spatial resolution surface reflectance images, from microsatellites PanetDove (PD), were used (Planet Team, 2017). PD constellation of microsatellites provide a daily overpass coverage. Only cloud free images were used. PD is a CubeSat 3U form factor (10 cm × 10 cm × 30 cm) microsatellite constellation operated by Planet, Inc. The PD constellation consists of about 130+ satellites, with the capability to image the entire Earth's land surface on a daily basis. The PD satellites have four spectral bands; Blue (B, 455-515 nm), Green (G, 500-590 nm), Red (R, 590-670 nm), and Near Infra-Red (NIR, 780-860 nm). These have a nominal Ground Sampling Distance (GSD) of 3 m at nadir and positional accuracy of < 10 m RMSE (Planet Team, 2019). These images are atmospherically corrected to 'Below of the Atmosphere' (BOA) or surface reflectance, which provides more consistency across time and location localized atmospheric conditions while minimizing uncertainty in the spectral response (Planet Team, 2020). Nineteen (19) PlanetScope images were used (July-September, 2020) to obtain surface reflectance, vegetation indices, and other derived variables. However, PD microsatellites do not carry a thermal camera to characterize the maize canopy surface temperature. For this reason, T_s data from fixed (ground-based) IRTs installed in the field were used. Further details can be found in Chávez (2021).

Figure 4. Irrigation Innovation Consortium research site near Fort Collins, Colorado, USA

3. Results

3.1 Sprinkler Irrigated Cotton Case

During the Cotton growth period, lysimeter measured ET_a varied from approximately 1.6 to 12 mm d^{-1} (Figure 5). This high-end cotton evapotranspiration rate was due to the highly advective conditions of the site. The evaluation of ET_a estimates, derived from the EB and T_o from Equation 2, was performed with lysimeter-based ET_a daily rates (Figure 5).

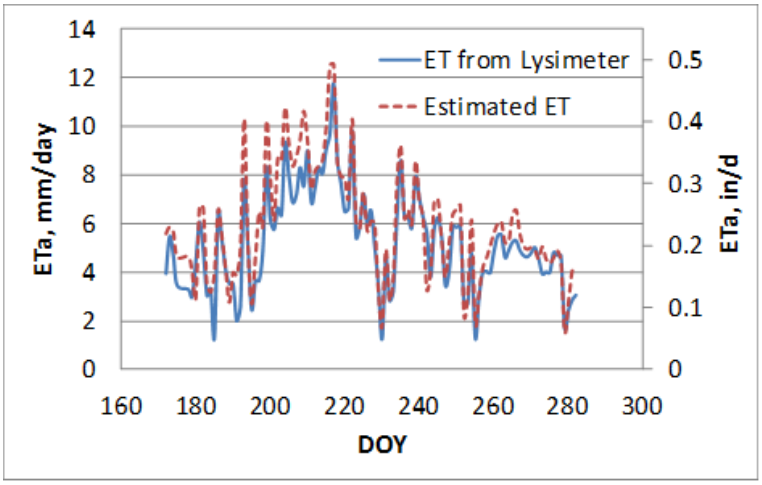

Figure 5. Cotton 2008 campaign daily ET_a measured (full line) and estimated (dashed line) from the USDA ARS CPRL, Bushland, Texas, USA

The evaluation indicated that the cotton ET_a estimation errors (MBE±RMSE) were 0.67±1.07 mm d^{-1} or 9.8±15.7% of normalized error (using mean measured ET values). This result is considered good given the full irrigation conditions and the environment (highly advective semi-arid region) in Texas that were very different from the conditions (humid, rainfed agriculture) encountered in Iowa where Equation 2 was developed.

3.2 Furrow Irrigated Maize Case—Rocky Ford, Colorado, USA

Resulting estimated maize ET_a values were evaluated with ET_a data from the large weighing lysimeter. Results indicate that the ET_a estimation errors (MBE±RMSE) were 0.28±0.52 mm d^{-1} or 3.9±7.5%. This result shows a small estimation errors, which is exceptional considering that the T_o model from Equation 2 was develop using data from a rainfed maize grown in a semi-humid climate, much different from the somewhat advective conditions encountered at the AVRC in Rocky Ford, Colorado. Figure 6 below illustrates the linear regression curve fitted to

the ET_a data (x-axis lysimeter measured and y-axis estimated), depicting some over estimation of ET_a in the range of 5.5-6.5 mm d^{-1}, for furrow irrigated maize.

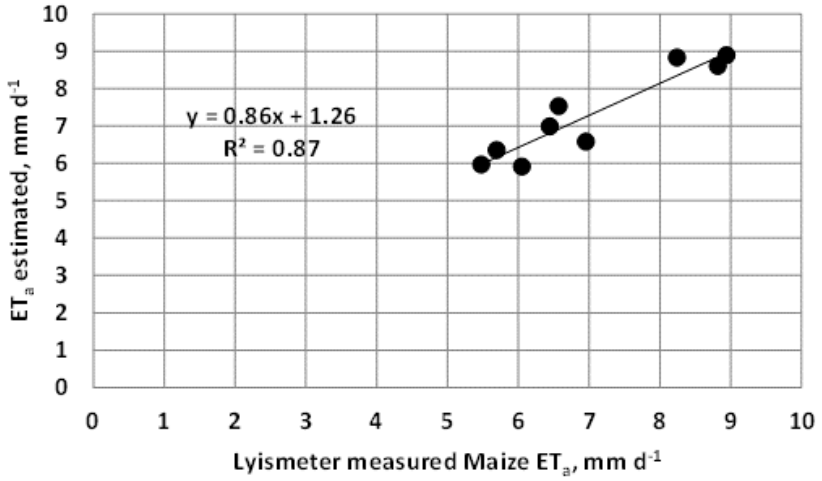

Figure 6. Maize ET_a (measured vs. estimated) evaluation. Data collected at the CSU AVRC research facility near Rocky Ford, Colorado, USA

3.3 Furrow Irrigated Maize—Fort Collins, Colorado, USA

Figure 7 below shows a true color (RGB) picture (left) of the maize grown at the IIC-HQ. The picture was taken with an unmanned aerial system (UAS), while the map shown on the 'right' hand side of Figure (7) depicts PlanetDove microsatellite-based NDVI values from the maize field during August 4th, 2020. NDVI is the "Normalized Difference Vegetation Index" equal to [NIR – R]/[NIR + R]; where NIR and R are surface reflectance values in the Near Infra-red and Red bands, respectively. For the most part, the maize biomass was homogeneous throughout the entire field as per the NDVI distributed values shown in Figure (7).

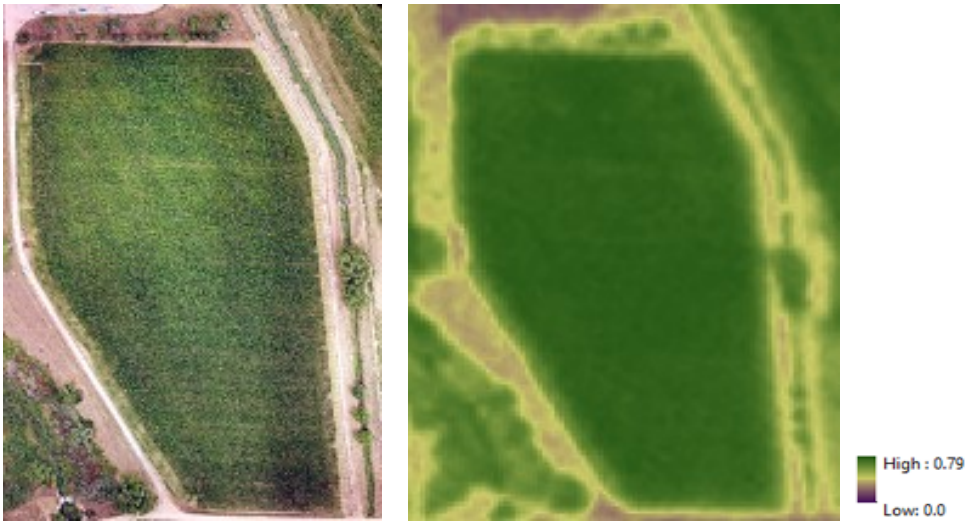

Figure 7. IIC-HQ west field depicting a maize field true color map (left), and an NDVI map (right) derived from a PlanetScope multispectral image acquired on 4 August 2020

Figure 8 below shows the linear regression between EC-based ET_a and estimated ET_a (through Equations 5-8 and the EB method); where some scatter is apparent at low and high ET_a rates (1-2 and 4.2-5.4 mm d^{-1}, respectively), while there is little scatter (better agreement) for medium ET_a rate values (~3.5-3.8 mm d^{-1}). Further, the ET_a evaluation yielded estimation errors of 0.12±0.78 mm d^{-1} or 3.2±20.7%. This result shows rather a larger than

expected ET_a overestimation for the surface irrigated maize case. One plausible reason may be the mismatch of footprints between the PlanetScope multispectral image pixel size (3 m) and the IRT readings footprint (~1m), the furrow irrigation sets (number of furrows per set and number of irrigation sets per day), and calibration of the Planet multispectral images.

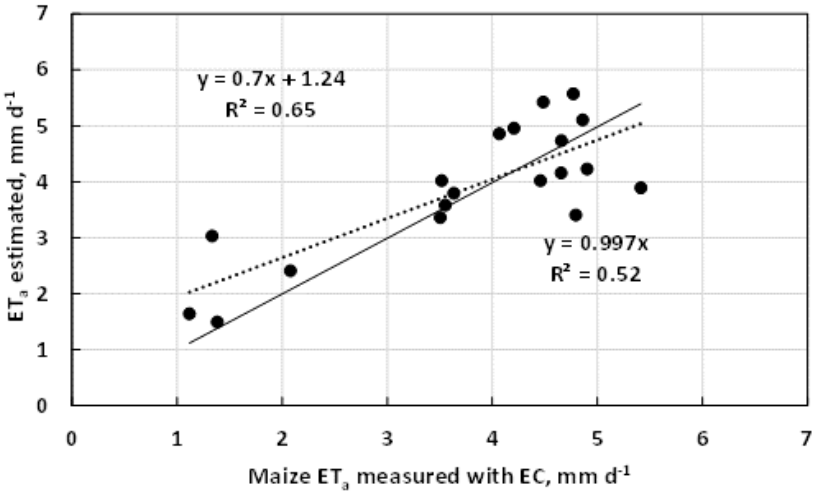

Figure 8. Linear regression plot between EC-based ET_a and T_o-based estimated maize ET_a for a research field near Fort Collins, Colorado, USA

4. Discussion

Actual crop evapotranspiration estimated for the fully irrigated cotton (in Texas) field resulted with relative errors of 9.8±15.7%. This error is considered acceptable given the fact that most daily ET_a models present an accuracy of about 15-20% of RMSE and that the aerodynamic temperature approach used in the estimation of ET_a was developed under different surface and environmental conditions. Equation 2 was developed to estimate T_o for rainfed maize subject to a semi-humid climate with relative errors of -2.7±11.7%. Further, the maize fields displayed periods of water stressed during the field data collection in Iowa, while the cotton field in Texas was not water stressed. Moreover, the irrigated cotton was subject to very advective conditions that added energy (horizontally) to the local vertical exchange of energy fluxes increasing the cotton ET_a rate higher than the values encountered in Iowa for the maize crop. Therefore, using Equation 2 to estimate T_o for cotton seems feasible although a local calibration of the T_o model may improve EB-based ET_a estimates. For this application case, the remote sensing data used as input in the simplified energy balance originated from a fixed stationary infra-red thermometer and a roaming handheld multispectral radiometer EXOTECH.

In the case of the fully (furrow) irrigated maize field from Rocky Ford, Colorado, ET_a was estimated with relative errors of 3.9±7.5%. This is considered an excellent result when compared to rainfed maize ET_a estimate errors of -2.7±11.7%, and considering the fact that the maize field in southeastern Colorado was also subject to advective conditions that promoted larger ET_a rates than in Iowa. This result may be evidence of the regional transferability, of the T_o model presented in Equation 2, from a semi-humid to a semi-arid region. In the case of the irrigated maize in southeastern Colorado, remote sensing data were also collected using a fixed IRT and a roaming multispectral radiometer (MSR5, CropScan, Rochester, Minnesota, USA); while Equation 2 was developed using RS data from an airborne system.

Finally, for the fully (furrow) irrigated maize grown near Fort Collins, Colorado, errors in the estimation of ET_a, using updated T_o models (Equations 5-8), were larger than errors obtained for rainfed maize in central Iowa and in southeastern Colorado for fully irrigated maize; and larger than ET_a errors obtained for drip irrigated (fully and deficit) maize near Greeley, Colorado. In this case, multispectral remote sensing inputs (surface reflectance in the R and NIR bands) were from a microsatellite and not from handheld radiometers. Both the footprints and radiometry of these sensors/platforms (*i.e.*, handheld and spaceborne) are different and seem to affect the accuracy of ET_a estimates. For instance, when the size of the microsatellite imagery pixel size does not much that of the IRT footprint, and there is local heterogeneity on crop stands (different crop height, fractional cover, LAI), then the

estimation of ET_a may not be that accurate. Further, the radiometric calibration of the PlanetScope reflectance images may not have been accurate and consistent. On this topic, regarding the quality of the Planet microsatellite images, Frazier and Hemingway (2021) stated the following "...the variation in radiometric and geometric quality compared to traditional platforms (*i.e.*, Landsat, MODIS, etc.) means the images are not always 'analysis ready' upon download.,," Meaning that further calibration is needed due to the lack of consistent good radiometric/geometric calibration. Earlier Latte and Lejeune (2020) highlighted the need of PlanetScope imagery normalization (calibration) to Sentinel-2 high quality imagery radiometric level due to frequent inconsistencies of PlanetScope microsatellites' radiometric quality. In fact, Planet Inc., started offering harmonized or normalized (to Sentinel2) images in March of 2022.

Thus, this study assessed the accuracy in the estimation of daily actual crop evapotranspiration rates through the use of the surface aerodynamic temperature approach in the energy balance method. Several aerodynamic temperature models have been calibrated for specific crops and environmental conditions. Those calibrated T_e models have resulted in accurate ET_a estimates for the locations where the models were developed for. Nevertheless, there seems that the surface aerodynamic temperature approach may be transferable to different climatic regions and crop types resulting in acceptable ET_a estimates. However, local calibration may be required to improve ET_a estimation results. Further, the aerodynamic temperature model is more accurate when applied using remote sensing input data collected with similar sensors/instruments as those used in the development of the T_o model. In the application cases presented in this study, the aerodynamic temperature model applied using multispectral and thermal data from proximal remote sensing devices (handheld and fixed sensors) produced more accurate ET_a rates than when using input data from microsatellites that may have experienced inconsistent imagery pixel radiometric calibration. This result highlights the need to evaluate the quality of satellite images using properly calibrated ground-based radiometers, and if needed develop local calibrations for each satellite overpass/scene. Still, the combination of daily microsatellite multispectral images and ground-based thermal data is promising for daily mapping of ET_a.

Even though the use of T_o models is promising, for the easier mapping of ET_a, further studies are needed to turn the approach operational and applicable at larger spatial (regional) scales on a daily basis. For instance, determining the effects of RS input data of different pixel sizes and radiometry (e.g., Landsat 8 and 9, Sentinel2, MODIS, PlanetDove harmonized) on ET_a is needed, as well as incorporating the different crop structures and their interaction with wind directional angle of attack, for a wide range of crop types and plating densities and spacing.

Acknowledgements

We are grateful for the financial support provided by the National Science Foundation (NSF Award 2120906). Our gratitude goes to the following individuals who participated facilitating or collecting data and/or processing data: Dr. Terry Howell, Karen Copeland, Brenna Mefford, Edson Costa, Lane Simmons, Dr. Mike Bartolo, Dr. Allan Andales, and A. J. Brown.

References

Bastiaanssen, W. G. M., Menenti, M., Feddes, R. A., & Holtslag, A. A. M. (1998), A remote sensing surface energy balance algorithm for land (SEBAL). 1. Formulation. *J. Hydrol., 212-213*, 198-212. https://doi.org/10.1016/S0022-1694(98)00253-4

Brest, C. L., & Goward S. N. (1987). Driving surface albedo measurements from narrow band satellite data. *Int. J. Remote Sens., 8*, 351-367. https://doi.org/10.1080/01431168708948646

Brunsell, N. A., & Gillies, R. (2002). Incorporating surface emissivity into a thermal atmospheric correction. *Photogramm. Eng. Remote Sens. J., 68*, 1263-1269.

Brutsaert, W. (1975). On a drivable formula for long-wave radiation from clear skies. *Water Resour. Res., 11*, 742-744. https://doi.org/10.1029/WR011i005p00742

Carrasco-Benavides, M., Ortega-Farías, S., Morales-Salinas, L., Poblete-Echeverría, C., & Chávez, J. L. (2017). Calibration and validation of an aerodynamic method to estimate the spatial variability of sensible and latent heat fluxes over a drip-irrigated Merlot vineyard. *International Journal of Remote Sensing, 38*(24), 7473-7496. https://doi.org/10.1080/01431161.2017.1317943

Chávez J. L., Howell, T. A., Gowda, P. H., Copeland, K. S., & Prueger, J. H. (2010). Surface aerodynamic temperature modeling over rainfed cotton. *Transactions of ASABE, 53*(3), 759-767.

Chávez, J. L. (2021). *Satellite and UAS Imagery Use to Implement Timely Irrigation Strategies* (Final project report submitted to the Irrigation Innovation Consortium (IIC), Project 7, September 2021).

Chávez, J. L., Gowda, P. H., Howell, T. A., Garcia, L. A., Copeland, K. S., & Neale, C. M. U. (2012). ET mapping with high resolution airborne remote sensing data in an advective semi-arid environment. (ASCE) *Journal of Irrigation and Drainage Engineering, 138*(5), 416-423. https://doi.org/10.1061/(ASCE)IR. 1943-4774.0000417

Chávez, J. L., Howell, T. A., & Copeland, K. S. (2009). Evaluating eddy covariance cotton ET measurements in an advective environment with weighing lysimeters. *Irrigation Science, 28*, 35-50. https://doi.org/10.1007/s00271-009-0179-7

Chávez, J. L., Neale, C. M. U., Hipps, L. E., Prueger, J. H., & Kustas, W. P. (2005). Comparing aircraft-based remotely sensed energy balance fluxes with eddy covariance tower data using heat flux source area functions. *Journal of Hydrometeorology, 6*(6), 923-940. https://doi.org/10.1175/JHM467.1

Chávez, J. L., Neale, C. M. U., Prueger, J. H., & Kustas, W. P. (2008). Daily Evapotranspiration estimates from extrapolating instantaneous airborne remote sensing ET values. *Irrigation Science, 27*, 67-81. https://doi.org/10.1007/s00271-008-0122-3

Chehbouni, A., Lo Seen, D., Njoku, E. G., & Monteny, B. M. (1996). Examination of the difference between radiative and aerodynamic surface temperature over sparsely vegetated surfaces. *Remote Sensing of the Environment, 58*, 177-186. https://doi.org/10.1016/S0034-4257(96)00037-5

Costa-Filho, E., Chávez, J. L., Zhang, H., & Andales, A. (2021). An Optimized Surface Aerodynamic Temperature Approach to Estimate Maize Sensible Heat Flux and Evapotranspiration. *Agricultural and Forest Meteorology, 311*, 108683. https://doi.org/10.1016/j.agrformet.2021.108683

Frazier, A. E., & Hemingway, B. L. (2021). A Technical Review of Planet Smallsat Data: Practical Considerations for Processing and Using PlanetScope Imagery. *Remote Sensing, 13*, 3930. https://doi.org/10.3390/rs13193930

Gowda, P. H., Chavez, J. L., Colaizzi, P. D., Evett, S. R., Howell, T. A., & Tolk, J. A. (2008). ET mapping for agricultural water management: Present status and challenges. *Irrigation Science, 26*(3), 223-237. https://doi.org/10.1007/s00271-007-0088-6

Kustas, W. P., & Norman, J. M. (1996). Use of remote sensing for evapotranspiration monitoring over land surfaces. *Hydrologic Sciences, 41*(4), 495-516. https://doi.org/10.1080/02626669609491522

Kustas, W. P., Choudhury, B. J., Moran, M. S., Reginato, R. J., & Jackson, R. D. (1989). Determination of sensible heat flux over sparse canopy using thermal infrared data. *Agricultural and Forest Meteorology, 44*, 197-216. https://doi.org/10.1016/0168-1923(89)90017-8

Latte, N., & Lejeune, P. (2020). PlanetScope Radiometric Normalization and Sentinel-2 Super-Resolution (2.5 m): A Straightforward Spectral-Spatial Fusion of Multi-Satellite Multi-Sensor Images Using Residual Convolutional Neural Networks. *Remote Sensing, 12*, 2366. https://doi.org/10.3390/rs12152366

Mahrt, L., & Vickers, D. (2004). Bulk formulation of the surface heat flux. *Boundary Layer Meteorology, 110*(3), 357-379. https://doi.org/10.1023/B:BOUN.0000007244.42320.1e

Planet Team. (2017). *Planet Application Program Interface: In Space for Life on Earth*. San Francisco, CA. Retrieved from https://api.planet.com

Planet Team. (2019). *Planet imagery product specifications*. Planet Inc. Accessed 07.05.2019.

Planet Team. (2020). *Planet surface reflectance product v2*. Planet Inc. Accessed 08.25.2020.

Rambikur, E., & Chávez, J. L. (2014). Assessing Inter-Sensor Variability and Sensible Heat Flux Derivation Accuracy for a Large Aperture Scintillometer. *Sensors, 14*(2), 2150-2170. https://doi.org/10.3390/s140202150

Wenbin, M., Zhongming, C., Linsheng, S., Wenliang, G., Xiuling, L., Tingrong, Y., … Xiurong, Y. (2004). A scheme for pixel-scale aerodynamic surface temperature over hilly land. *Advances in Atmospheric Sciences, 21*(1), 125-131. https://doi.org/10.1007/BF02915686

Appendix A

Net Radiation and Soil Heat Flux Modeling

Net radiation (W/m^2) is modeled based on Equation A1 below.

$$R_n = (1 - \alpha)\cdot R_s + \varepsilon_a\ \sigma\ T_a^4 - \varepsilon_s\ \sigma\ T_s^4 \quad (A1)$$

where, α is surface albedo, R_s is incoming shortwave radiation (W/m^2), ε_a is atmospheric thermal emissivity, ε_s is surface thermal emissivity, T_a is air temperature (K) and T_s is radiometric surface temperatures (K), while σ is the Stefan-Boltzmann constant ($5.67 \times 10^{-8}\ W/m^2/K^4$).

Surface albedo is estimated using the Brest and Goward (1987) approach.

$$\alpha = 0.512\cdot RED + 0.418\cdot NIR \quad (A2)$$

where, RED and NIR are surface reflectance values in the Red and Near Infra−Red bands of the electromagnetic spectrum.

Air or atmospheric emissivity is calculated using the Brutsaert (1975) approach.

$$\varepsilon_a = 1.24\cdot(e_a/T_a)^{1/7} \quad (A3)$$

where, e_a is the actual vapor pressure (mb) and T_a is air temperature in K.

Surface thermal emissivity is calculated using Brunsell and Gillies (2002).

$$\varepsilon_s = 0.98\cdot f_c + 0.92\cdot(1 - f_c) \quad (A4)$$

where, f_c is the fractional vegetation cover.

Soil heat flux (W/m^2) is estimated using Bastiaanssen et al. (1998) approach.

$$G/R_n = (T_s/\alpha)\cdot(0.0038\ \alpha + 0.0074\ \alpha^2)\cdot(1 - 0.98\ NDVI^4) \quad (A5)$$

where, NDVI is the Normilized Difference Vegetation Index.